FEA Prediction of Off-Road Tire Temperature Distribution

W. Nyaaba, S. Frimpong, G. Somua-Gyimah and G. Galecki

Department of Mining and Nuclear Engineering

Missouri University of Science and Technology, Rolla, Missouri, USA.

Abstract: *Excessive heat generation and retention in ultra-large dump truck tires is among the most common causes of tire failures in the surface mining industry. Accurate prediction of an operating tire temperature profile involves the use of advanced numerical models and solution schemes to mimic the complete elastomeric materials response to operating conditions. The internally generated heat in a tire is a function of its viscoelastic energy dissipation during rolling. Previous research studies have inaccurately predicted off-the-road (OTR) tire heat generation rates and temperatures by the use of linear viscoelasticity to approximate the rather nonlinear viscoelastic rubber material. This paper presents an accurate approach to predicting OTR tire temperature distributions taking into account the true mechanical response of the filled rubber compounds used in tires. Rubber nonlinear viscoelasticity was modeled using the recently implemented parallel rheological framework (PRF) in Abaqus. Stress relaxation test data for two regional compounds (tread and carcass) were used to calibrate the PRF material model parameters using the data matching component of Isight. A fully coupled thermal-stress analysis procedure in Abaqus/Explicit was adopted to compare temperature distributions of a typical Michelin 59/80R63 tire modeled using two material theories: (i) linear viscoelasticity, and (ii) nonlinear viscoelasticity. The results obtained show that tire temperature distributions are more accurately predicted by the PRF material model than by the Prony series model.*

Keywords: Off-The-Road Tire, Nonlinear Viscoelasticity, Temperature, Rubber, Isight, Parallel Rheological Framework.

1. Introduction

The current economic environment and commodity market depression require that the mining industry focuses on minimizing costs while improving mine safety and productivity. Tire service and replacement costs are key contributors to the whole-mine cost centers and, thus need to be given adequate attention. Tire heat failure is among the most common causes of their maintenance and/or replacement in the industry. Practical measures including the tire ton-mile-per-hour (TMPH) monitoring program have been used to predict tire temperature limits for given jobs but the problem of tire heat-related failures still remains a challenge to the industry. The elastomeric matrix of a tire is reinforced with both particulate and fibrous inclusions to improve its stiffness, rupture energy, fatigue resistance, tear and tensile strength properties.

The interspersed particulate inclusions, predominantly carbon-black and silica, give the filled compound nonlinear response characteristics which are primarily driven by the physical and chemical processes occurring within it at varying strain levels. Such processes include extreme mismatch in stiffness between the reinforcing particles and the near-incompressible nonlinear viscoelastic matrix, particle debonding, and void growth (Areias, 2008). In modeling the highly nonlinear rate dependent filled compounds in pneumatic tires, continuum-based models have been used with varying numerical implementation complexities (Bergstrom, 2001; Drozdov, 1998; Drozdov, 2001; and Lapczyk, 2012). Consequently, most researchers have over the past decades relied on the linear viscoelastic model implemented in commercial FE packages to approximate the rather nonlinear viscoelastic behavior of the filled rubber compounds used in tires. Part of the reasons for the premature tire heat removal among mining haulage trucks could be ascribed to the erroneous predictions of acceptable tire operating temperature limits from the theory of linear viscoelasticity.

Accurately predicting an operating tire heat generation and corresponding temperature rise will involve the use of an appropriate model that captures the nonlinear response of the filled compound as functions of strain and time (Nandi, 2014). The internally generated heat in a tire is a function of its viscous dissipation energy during rolling. Thus, this paper focuses on using the parallel rheological framework (PRF) model in Abaqus (Abaqus, 2014) to model the highly nonlinear rate-dependent behavior of the filled rubber compounds. The PRF material model is capable of capturing the complete nonlinear response of rubber viscoelasticity through its use of multiple elastic and viscous networks in its framework.

In obtaining the PRF model parameters, the data matching capability of the framework package Isight was used. Total loaded truck weight, cavity air pressure, ambient temperature, and travel speed were among the common operating conditions considered in the paper. A fully coupled thermal stress solution scheme based on the finite element method is adopted in this work to compare temperature distributions of a typical Michelin 59/80R63 tire modeled using two approaches: (i) linear viscoelasticity, and (ii) nonlinear viscoelasticity.

2. Tire Geometry and FE Model

The Michelin 59/80R63 tire is designed for trucks capable of handling nominal payloads of about 400 tons. The high load, high speed application tire is constructed of a single layer of super tensile strength steel body ply and six steel belt layers. A 2D axisymmetric model of the carcass and reinforcing plies were used in obtaining the full tire model in Abaqus. Figure 1 shows the assembly of the axisymmetric parts. Bilinear axisymmetric quadrilateral, reduced integration elements with twist degrees of freedom (CGAX4R and CGAX3R), were used to account for twist in the cords along the axisymmetric axis due to the anisotropy associated with fiber reinforcements (Kabe, 2000). The body ply and belt cord geometries were modeled as separate parts using the wire feature. Rebar layers defined in surface elements were used to approximate carcass reinforcements. The current model employed the embedded constraint option to define the body ply reinforcement since its local response were of little significance to the authors. However, the node sharing option through skin definitions was used to introduce the belt reinforcement.

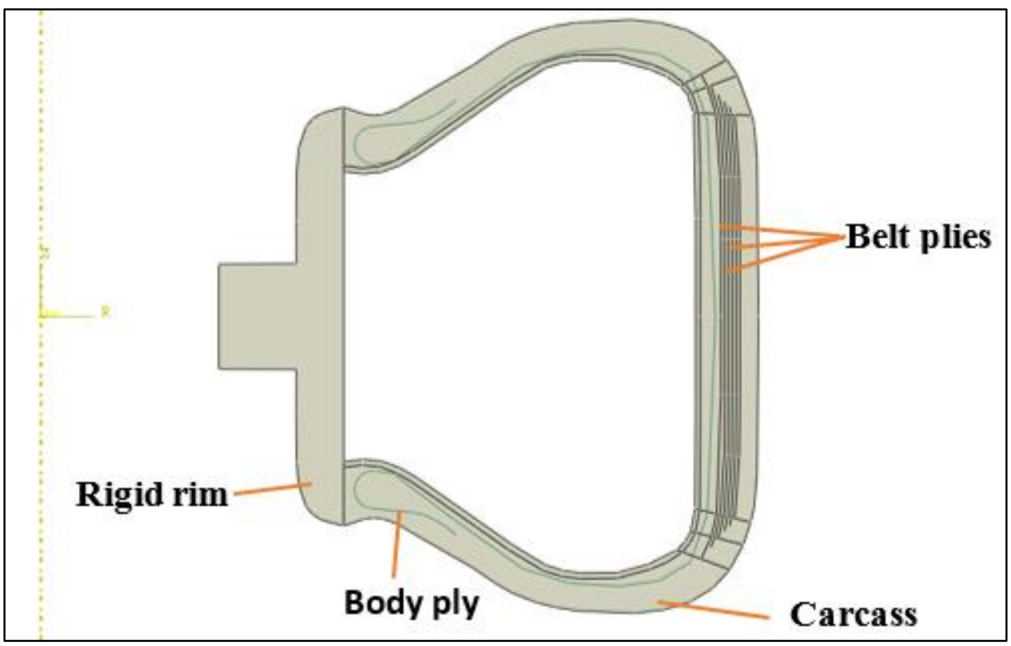

Figure 1. Axisymmetric model.

Introducing belt reinforcements in this manner allows inter-belt layer shearing to be assessed. Given the out-of-plane nature of the rebar layers, the 2-node SFMGAX1 with twist elements were selected for the rebar layers. Figure 2 shows the meshed geometry of the carcass. A total of 1930 elements were used in the axisymmetric model. The bead-rim contact region was approximated with rigid body constraints due to the high stiffness in the region. Thus, a rigid rim is defined with its reference point serving as the point of load/boundary condition application. The axisymmetric model was solved at tire cavity pressure of 0.7 MPa and fixed at the rim reference point. Using the symmetric model generation (SMG), revolve, and symmetric results transfer (SRT) options in Abaqus, the carcass sector model was obtained from revolving the axisymmetric model 15° about its symmetry axis. A separately meshed patterned tread block was tied to the sector model using tie constraints. The tied assembly, shown in Figure 3a, was fixed at the rim reference point through the encastre boundary condition option. An inflation step was defined in Abaqus/Standard to solve the tread-carcass sector model over a simulation time of 1 s.

A footprint analysis was further conducted using the full 3D model generated by revolving the 3D tread-sector model repetitively about the symmetry axis. The full 3D tire model used in the footprint step is shown in Figure 3b. A key advantage in using both SMG and SRT options is that results from the original model is always transferred to the new model to serve as the initial state of the new model. Results transfer is made possible only when a restart file is requested during the solution of the original model. It is also worth noting that uniform meshing was used throughout the full 3D model as the intention was to import the model into Abaqus/Explicit for dynamic rolling analysis. An analytical rigid surface was defined to represent the road contact surface in the model.

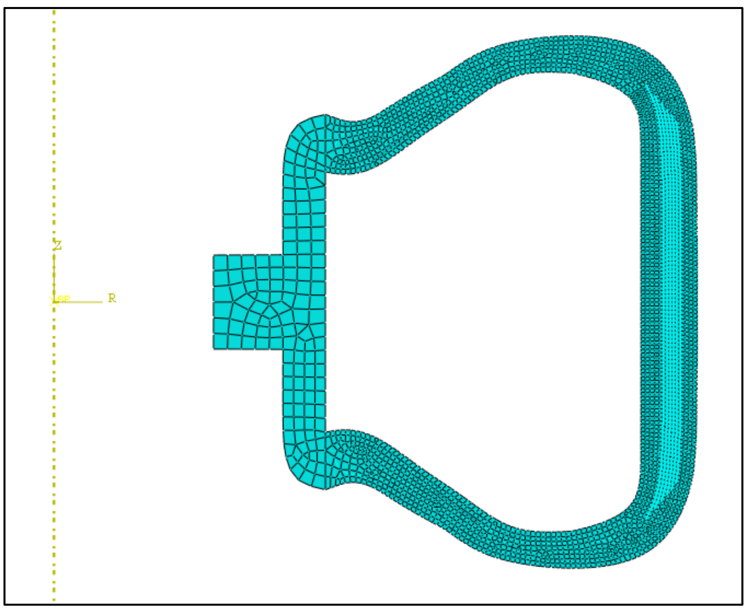

Figure 2. Axisymmetric carcass mesh.

Given the scarcity of tire material data, rubber compound data obtained from the literature (Yang, 2011) was used for the present model. Two regional compounds: tread and carcass, with properties summarized in Table 1, were assigned to the respective regions to complete the initial material definition of the model. The Yeoh's hyperelastic potential appeared to best fit the uniaxial tension experimental data provided in Yang (2011). The reinforcing elements were assigned linear elastic properties. Table 2 shows the material and section definitions of the rebar layers used in the model. The belt structure, comprising six layers of cord reinforcements, has four working belts interposed between the innermost (transition) belt and the outer penetration protection belt.

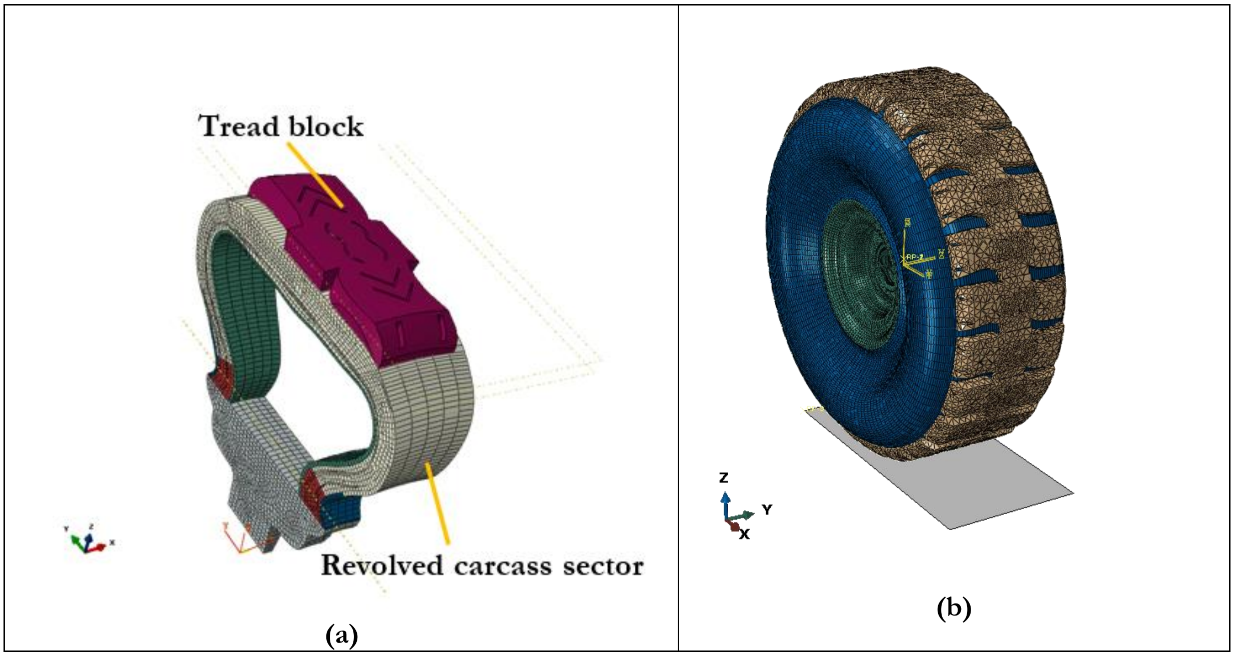

Figure 3. Revolved models of: (a) carcass cross-section, and (b) carcass sector.

Two viscoelastic models: linear and nonlinear were defined for two models of the same tire. This was done to compare the heat dissipations and nodal temperatures from both models. As presented in Nandi (2014), linear viscoelastic theory is implemented in Abaqus as a Prony series expansion of the dimensionless relaxation modulus in equation (1).

$$g_R(t) = 1 - \sum_{i=1}^{N} \bar{g}_i^p \left(1 - e^{-t/\tau_i^G}\right), \tag{1}$$

$N, \tau_i^G, \overline{g}_i^p, i = 1,2, \ldots, N$ are material constants and are presented in Table 1. Conversely, nonlinear viscoelasticity is implemented through the PRF model (Lapczyk, 2012), which is discussed in detail in section 3.

Table 1. Rubber material data.

Regions	C_{10} (MPa)	C_{20} (MPa)	C_{30} (MPa)	Density (kg/m^3)	Specific heat c_p 10^3 (kJ/kgK)	Thermal conductivity μ (W/mK)	Thermal expansion α $(1/℃)$	Relaxation Modulus		Relaxation time	
								g_1	g_2	τ_1	τ_2
Carcass	0.293	-0.0886	0.03714	1190	2.01	0.000153	7.70E-05	0.117	0.09	21.3	350.1
Tread	0.171	-0.0440	0.01738	1190	2.01	0.000153	7.70E-05	0.143	0.09	7.6	235.6

Table 2. Reinforcement section definitions.

Belt/Ply	Spacing	Orientation	Area (mm^2)

	(ends/mm)	(°)	
Transition Belt	31.4	65	2.7025
Working Belt 1	31.4	-22	2.7025
Working Belt 2	31.4	22	2.7025
Working Belt 3	31.4	-22	2.7025
Working Belt 4	31.4	22	2.7025
Penetration Protection	31.4	-22	2.7025
Ply	31.4	0	2.7025

3. The PRF Model

Researchers have discovered that filled rubber compounds exhibit nonlinear rate-dependent behavior when undergoing finite strain cycles (Bergström, 2000; Nandi, 2014; and Drozdov, 1998). Rubber nonlinear behavior can also be attributed to its large change in geometry as it deforms. At the molecular level, Nandi (2014) pointed out that realignment in elastomer chains during the loading regime results in a nonlinear response that varies with strain levels and time. Vulcanized rubber is hyperelastic and shows a substantial amount of viscoelasticity requiring a material model capable of accounting for both effects. The PRF model tends to meet the modeling requirement of filled rubber by allowing multiple parallel elastic and viscoelastic networks to be defined in its framework. The framework (Figure 4) consists of multiple elastic and viscoelastic networks connected in parallel. Note that N is an arbitrary number of viscoelastic networks in the framework. In order not to allow complete stress relaxation in the material over time, a purely elastic or equilibrium network (network 0 in Figure 4) is defined. Each viscoelastic network assumes a multiplicative split of the deformation gradient into an elastic component and viscous component (Lapczyk, 2012). The elastic response of each network is assumed to be determined by a hyperelastic potential where the Yeoh's model was used in this paper.

Viscous dissipation energy resulting from rubber hysteresis is converted into heat. A creep potential is used to describe the evolution of the viscous part of the deformation gradient. Given a specified creep potential G^{cr}, a flow rule, and an evolution law (power-law strain hardening model), the viscous component of the deformation gradient can be characterized. The mathematical underpinning of the PRF model is detailed in Lapczyk (2012) and Nandi (2014). Using the PRF model implemented in Abaqus requires that the model's parameters are calibrated. The calibration approach in Nandi (2014) was followed to compute the PRF parameters from a stress relaxation test data. Published stress relaxation test data at 20% strain level (Yang, 2011) was used for the tread and carcass regions of the tire. Figure 5a-b shows plots of the normalized stress relaxation data obtained after Abaqus evaluation for Prony series parameters was conducted. The Prony series and the hyperelastic parameters are given in Table 1. The starting values of the PRF model parameters were derived from the Prony series parameters. As a requirement for the PRF model, the power law strain hardening model was used to incorporate the creep behavior of the rubber materials (Abaqus, 2014) as defined in equation (2).

$$\dot{\epsilon}^{cr} = \left(A\tilde{q}^{n}[(m+1)\,\epsilon^{cr}]^{m}\right)^{1/_{m+1}}, \qquad (2)$$

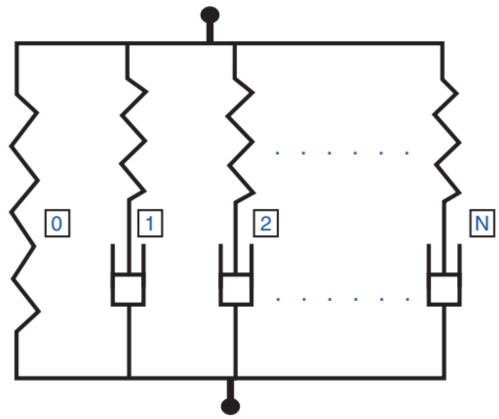

Figure 4. Schematic of the PRF model (Abaqus, 2014).

$\dot{\epsilon}^{cr}$ and ϵ^{cr} represent the equivalent creep strain rate and creep strain tensors, respectively. Note that A, m, and n are material constants whereas $\tilde{q}$ is the equivalent deviatoric Kirchhoff stress tensor. The linearized PRF power law strain hardening model parameters (starting values) were computed from the Prony series parameters according to the relations in equations (3) and (4).

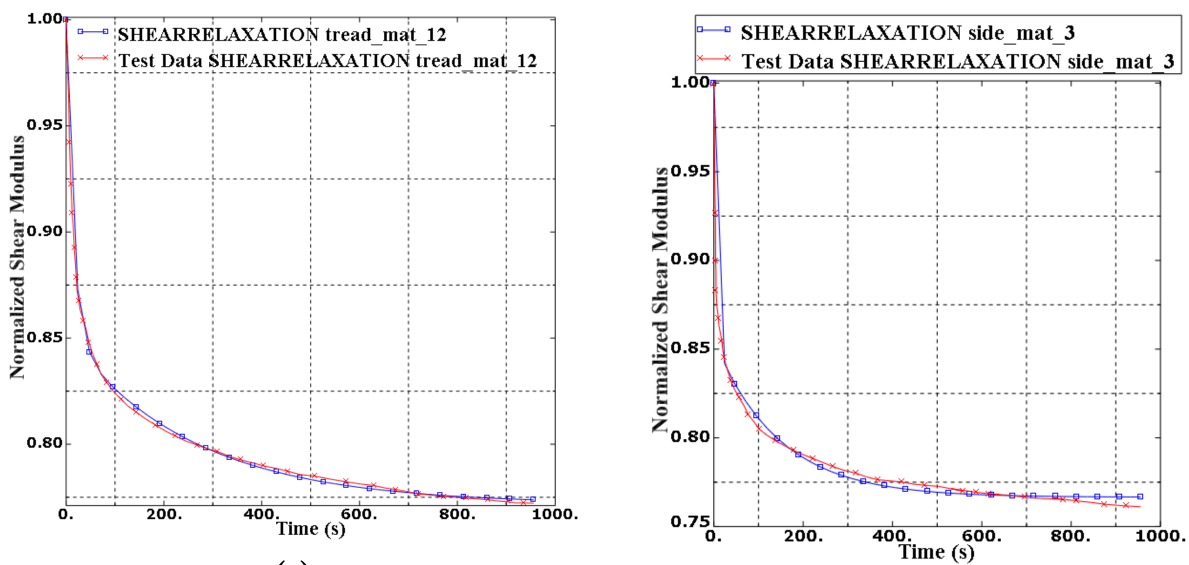

(a) (b)

Figure 5. Linear viscoelastic evaluation plots of (a) tread compound and (b) carcass compound.

$$SR_i = g_i \tag{3}$$

$$A_i = \frac{1}{(6 g_i t_i C_{10})} \tag{4}$$

The material constants: m_i and n_i are set to 0 and 1, respectively in the linearized PRF setup. SR_i is the stress ratio of the i^{th} viscoelastic network. Table 3 summarizes the initial linearized PRF model parameters for both tread and carcass compounds based on the Prony series and Yeoh's model parameters in Table 1.

Table 3. Linearized PRF model parameters for tread and carcass compounds.

Linearized Power Law Strain Hardening Parameters	Tread Compound	Carcass Compound
m_1	0.000	0.000
m_2	0.000	0.000
n_1	1.000	1.000
n_2	0.000	0.000
SR_1	0.1433	0.117
SR_2	0.090	0.090
A_1	0.895	0.228
A_2	0.046	0.0181
C_{10}	0.171	0.293
C_{20}	-0.044	-0.087
C_{30}	0.0174	0.037

Lastly, the linearized PRF model parameters were optimized in Isight 5.9-2 and Abaqus 6.14-1 using a unit-element cube model. Displacement controlled uniaxial tensile test was conducted using a visco analysis step to stretch the cube model in order to attain a strain of 65% over simulation time of 960 s. In applying the boundary conditions shown in Figure 6, inferior faces AFHD, ABEF, and ABCD, ABEF, and AFHD were constrained along their respective perpendicular directions x, y, and z, while the nodes of face BEGC were stretched along the x-direction. The PRF material model calibration was achieved by the data matching component in Isight. The workflow setup in Isight is shown in Figure 7. Here, both hyperelastic model coefficients and the linearized PRF model parameters served as starting values in the optimization component. The Hooke-Jeeves direct penalty algorithm was chosen to fit the simulation stress relaxation data to the measured stress relaxation data.

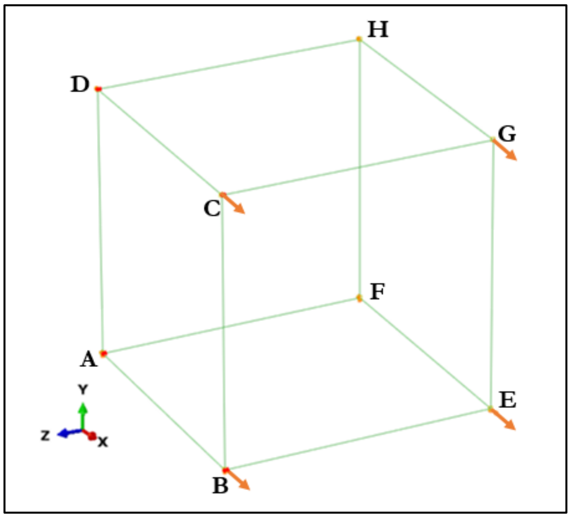

Figure 6. Cube with displacement boundary conditions.

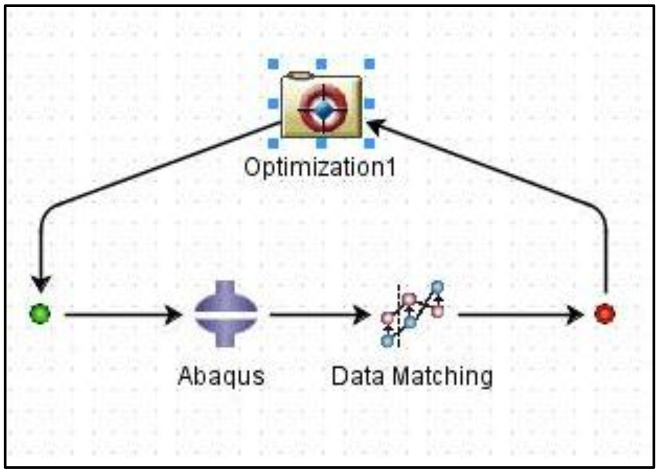

Figure 7. Isight workflow.

Figures 8 and 9 show results of the simulated linearized PRF model (starting values) and optimized PRF model stress relaxation response for both tread and carcass compounds, respectively. The optimized hyperelastic and PRF parameters are given in Table 4 below.

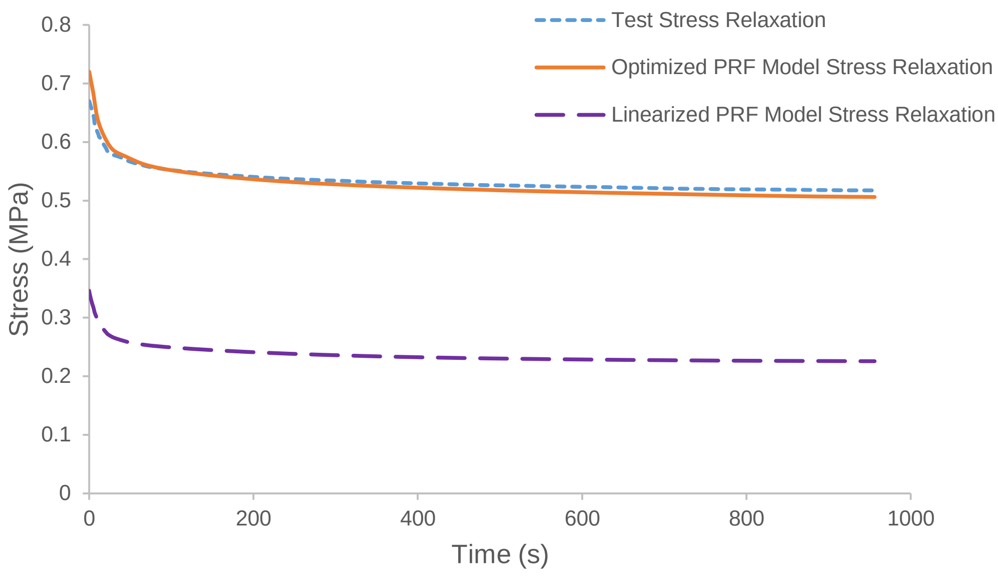

Figure 8. Tread compound simulation data vs test data.

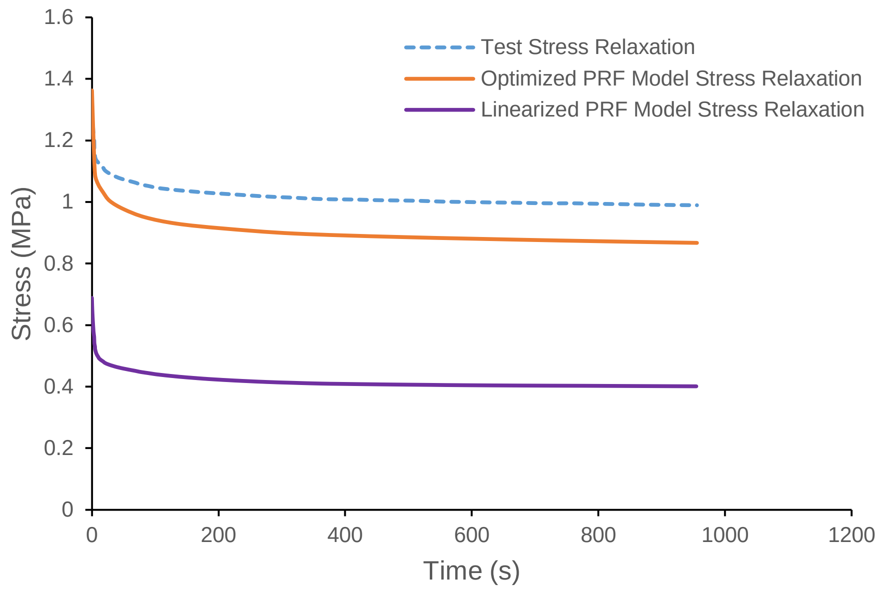

Figure 9. Carcass compound simulation data vs test data.

Table 4. Optimized PRF model parameters for tread and carcass compounds.

Optimized Power Law Strain Hardening Parameters	Tread Compound	Carcass Compound
m_1	-0.06	-0.060
m_2	-0.01	-0.079
n_1	3.000	4.000
n_2	3.000	4.000
SR_1	0.048	0.000
SR_2	0.000	0.000
A_1	0.033	0.955
A_2	0.030	0.044
C_{10}	0.162	0.298
C_{20}	0.056	0.014
C_{30}	0.000	0.037

The initial tire model hyperelastic and linear viscoelastic material definitions, in Table 1, were then changed to those in Table 4 in order to use the nonlinear viscoelastic model in the rolling analysis in section 4.

4. Transient Dynamic Rolling Analysis

A single-step straight-line rolling analysis was conducted in Abaqus/Explicit where a vertical load and velocity boundary conditions were specified at the rim center representing the wheel axle (Nyaaba, 2015). An analytical rigid surface was used to represent the road in the current analysis in order to offset the numerical cost otherwise incurred when a deformable road is used. A traction torque was applied around the wheel axle, as shown in Figure 10, at an angular velocity, ω, of 9.93 rad/s and a ground velocity, V, of 18775.68 mm/s (42 mph), which is the maximum recommended loaded travel speed of the CAT 797 series trucks. Thermal interactions defined through the surface film condition option were used to include the tire's outer surface interactions with cavity and ambient conditions. Thus, a constant convective film coefficient, h_c, is defined for all exposed surfaces in the model and it is given by the empirical relation (Li, 2012): $h_c = 5.9 + 3.7 v_a W/m^2$, where v_a is the relative air flow velocity between tire surface and its environment. Note that v_a used in the analysis was 18 m/s. A sink temperature of 24℃ was specified for both the tire inner and outer convective surfaces on the basis that contained air and ambient air temperatures were identical at the start of the analysis. A friction coefficient of 0.3 was assumed for the tread-road interaction.

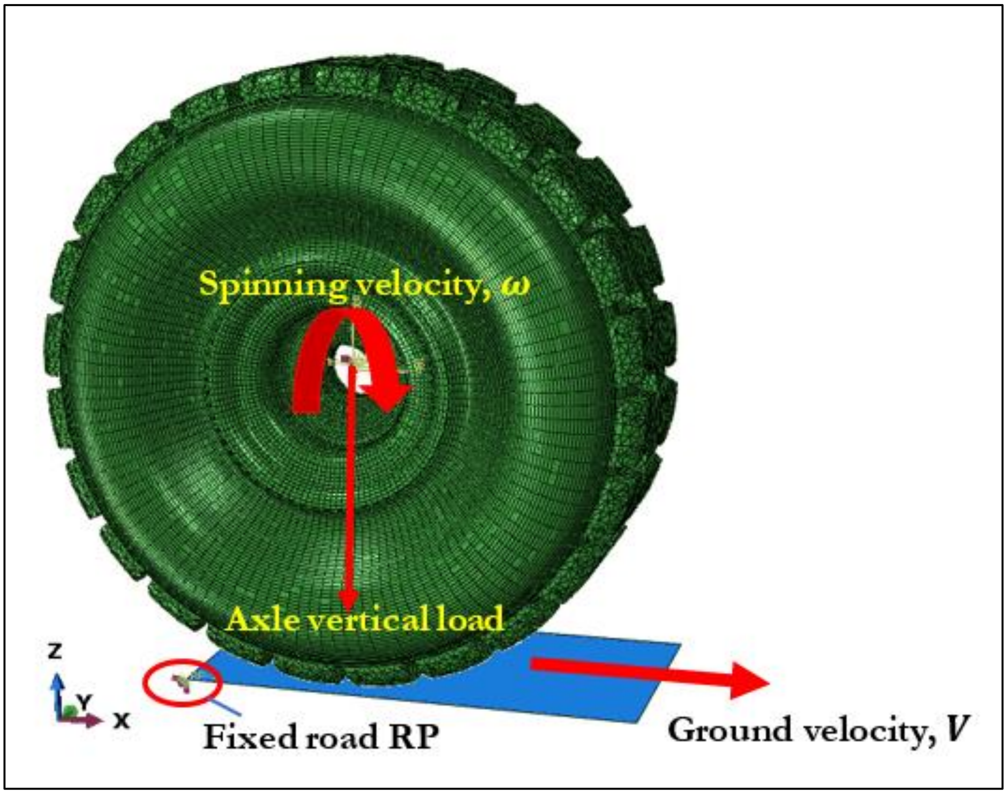

Figure 10. Load and boundary conditions.

A vertical load of 1.02 MN was applied at the axle reference point. The tire was simulated under a single ground speed condition at an inflation pressure of 700 kPa. A fully coupled temperature-displacement analysis procedure was adopted to investigate the differences in heat generation and corresponding temperature rise in two tire models that were only different in their representation of viscoelasticity. Without loss of generality, Model A refers to the tire model developed with Prony series representation of viscoelasticity whereas Model B is that defined with the PRF material model. Total simulation time for both analyses was 3 s.

To check for creep dissipation energy, element sets consisting of tread and sidewall elements were created in both models in which creep dissipation energy density (CENER) and creep dissipation energy (ALLCD) outputs were compared. Consistent with results reported in Nandi (2014), it was observed that Abaqus/Explicit outputs approximate results for creep dissipation energy with linear viscoelastic model as Model A shows zero ALLCD in Figures 11 and 12.

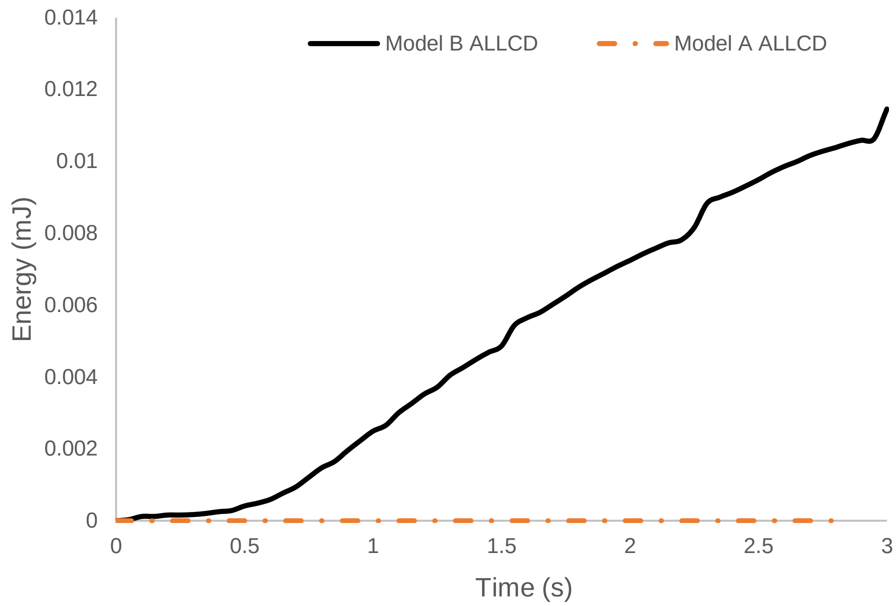

Figure 11. Sidewall element creep dissipation energy (ALLCD).

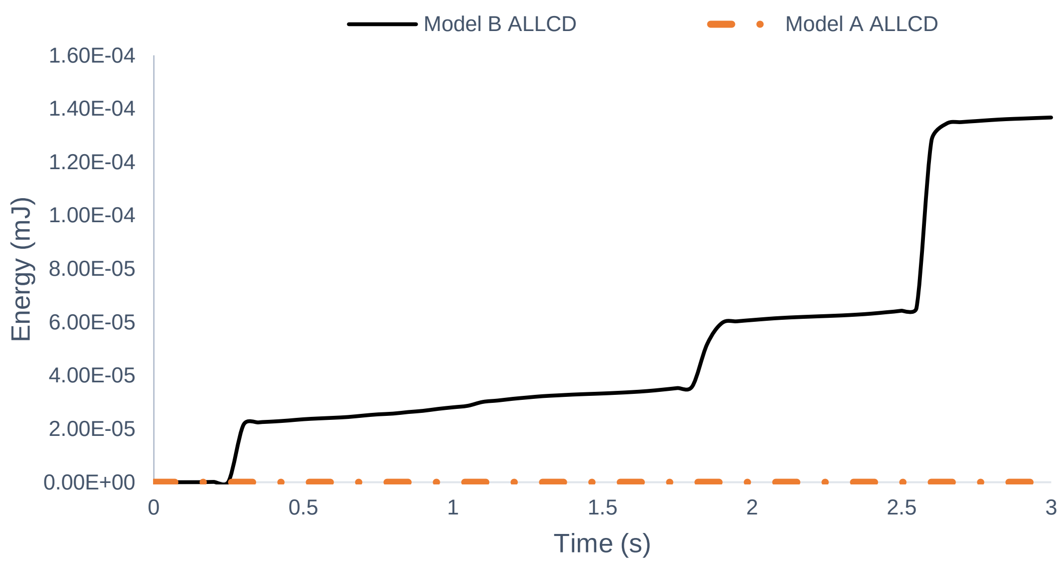

Figure 12. Tread element creep dissipation energy (ALLCD).

Creep dissipation energy resulting from rubber hysteresis in Model B was observed to increase in a step-wise manner in Figures 11 and 12. This trend could be explained by the cyclical loading routine at the ground contact, which results in a sudden rise in dissipation energy as the element enters the contact patch and plateaus as it exits out until the next entry. The correct estimate of ALLCD using the PRF model means temperatures resulting from Model B will be more accurate than those obtained from Model A. Contour plots of nodal temperatures are shown in Figures 13a-b. Model B shows a 50% decrease in temperature than that of Model A for the same simulation time. Thus, it suffices to conclude that temperature computations using the PRF material model is more accurate than temperatures obtained based on the theory of linear viscoelasticity.

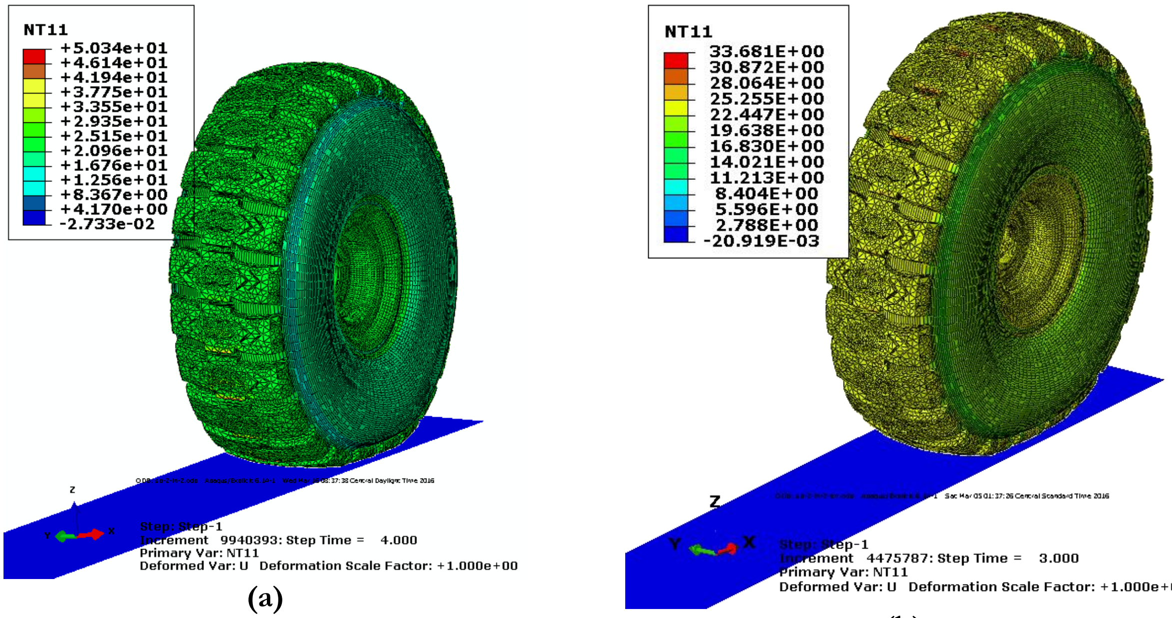

(a)

(b)

Figure 13. Contour plots of nodal temperatures of: (a) Linear viscoelastic model (A), and (b) PRF model (B).

Another interesting observation made was that higher nodal temperatures were found to occur in the tread elements whereas carcass elements showed low temperature values as depicted in Figure 14a-b. The reason for this large disparity could be partly attributed to the sub-optimum PRF model parameters obtained for the carcass compound. In Figure 9, it is clear that not a good fit was obtained between the optimized PRF simulation and test stress relaxation curves of the carcass compound. Conversely, the differences could also be ascribed to the addition of tread-road frictional energy dissipation. A fraction of the interfacial heat generated from frictional sliding was specified to enter the tread elements through the use of the gap heat generation option. Contact pressure contour plot of the tread is shown in Figure 15. Although there is no experimental data to compare the contact area with, the shape seems to show uniform contact pressure distribution on the road.

5. Conclusion

It has been established that filled rubber compounds used in tires exhibit nonlinear viscoelastic response when loaded, and thus, require a material model capable of capturing the material and geometric nonlinearities while accounting for viscous effects under varying strain levels and time. It has been shown, in this work, that the parallel rheological framework (PRF) model implemented in Abaqus is capable of meeting the modeling requirements of filled compounds. Two distinct models of the Michelin 59/80R63 tire have been analyzed each for linear and nonlinear viscoelastic response, particularly, in tire temperature predictions. The creep dissipation energy computation technique in the PRF model is more accurate than the technique in the linear viscoelastic model. Thus, temperature results from a model, which is based on the theory of nonlinear viscoelasticity and defined through the PRF material model, will always be more accurate than that defined by Prony series linear viscoelasticity. In addition, it has been shown that hyperelastic and Prony series terms are needed as starting values for the PRF model calibration which are then optimized using any available material calibration package. The data matching component of Isight has been proven to be useful in this regard. Frictional heat generation in the contact patch has been shown to contribute to the overall heat sources responsible for temperature rise in rolling tires.

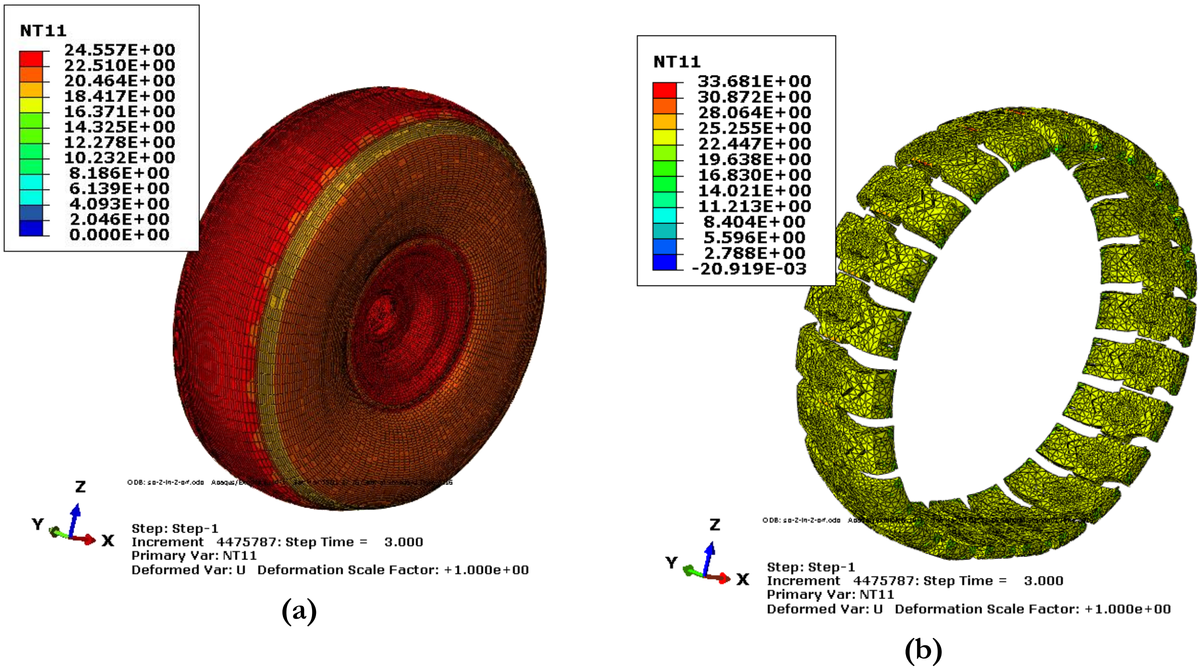

Figure 14. Nodal temperature distributions in: (a) carcass elements, and (b) tread elements.

6. Future Work

The authors wish to allow enough simulation time to reach steady state solutions in the future. It also appears sub-optimum PRF model parameters were used for the carcass region. This needs to be corrected to ensure accurate prediction of nonlinear viscoelastic behavior of the carcass elements.

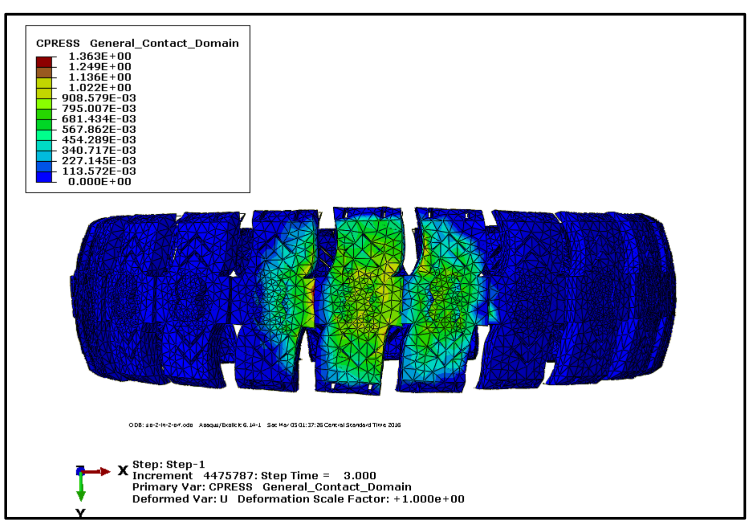

Figure 15. Footprint area showing contact pressures.

7. References

1. Abaqus Analysis User's Guide Volume III, Version 6.14-1, Dassault Systèmes Simulia Corp., Providence, RI.
2. Areias, P., & Matouš, K., "Finite element formulation for modeling nonlinear viscoelastic elastomers," Computer Methods in Applied Mechanics and Engineering, 197(51), 4702-4717, 2008.
3. Bergström, J. S., and Boyce, M. C., "Large strain time-dependent behavior of filled elastomers," Mechanics of materials, 32(11), 627-644, 2000.
4. Bergström, J. S., and Boyce, M. C., "Constitutive modeling of the time-dependent and cyclic loading of elastomers and application to soft biological tissues," Mechanics of materials, 33(9), 523-530, 2001.
5. Drozdov, A. D., "A model for the nonlinear viscoelastic response in polymers at finite strains," International journal of solids and structures, 35(18), 2315-2347, 1998.
6. Drozdov, Aleksey D., and Al Dorfmann. "Stress–strain relations in finite viscoelastoplasticity of rigid-rod networks: applications to the Mullins effect," Continuum Mechanics and Thermodynamics 13, no. 3, 183-205, 2001.
7. Kabe, K., & Koishi, M., "Tire cornering simulation using finite element analysis," Journal of Applied Polymer Science, 78(8), 1566-1572, 2000.
8. Lapczyk, I., J. A. Hurtado, and S. M. Govindarajan, "A Parallel Rheological Framework for Modeling Elastomers and Polymers," 182nd Technical Meeting of the Rubber Division of the American Chemical Society, Cincinnati, OH, October 2012.
9. Li, Y., Liu, W. Y., & Frimpong, S., "Effects of ambient temperature on stress, deformation and temperature of dump truck tire," Engineering Failure Analysis, 23, 55-62, 2012.
10. Nandi, B., Dalrymple, T., Yao, J., and Lapczyk, I., "Importance of Capturing Non-linear Viscoelastic Material Behavior in Tire Rolling Simulations," In *Presented at the* (Vol. 8, p. 10), 2014.
11. Nyaaba, W., Frimpong, S., and Gbadam E., "Thermo-mechanical Stress Loading and Deformation of OTR Dump Truck Tires in Surface Mining Operations" International Journal of Advanced and Innovative Research, 4(9), 138-140, 2015.
12. Yang, X., "Finite element analysis and experimental investigation of tyre characteristics for developing strain-based intelligent tire system*,"* Doctoral dissertation, University of Birmingham, 71-95, 2011.